International Journal of Heat and Fluid Flow 29 (2008) 1558–1566

Contents lists available at ScienceDirect

International Journal of Heat and Fluid Flow

journal homepage: www.elsevier.com/locate/ijhff

Study of heat-transfer on the surface of a circular cylinder in flow using an immersed-boundary method

N. Zhang [a,*], Z.C. Zheng [b], S. Eckels [b]

[a] Department of Engineering, McNeese State University, Lake Charles, LA 70609, USA
[b] Department of Mechanical and Nuclear Engineering, Kansas State University, Manhattan, KS 66506-5205, USA

ARTICLE INFO

Article history:
Received 21 March 2008
Received in revised form 17 July 2008
Accepted 29 August 2008
Available online 19 October 2008

Keywords:
Immersed-boundary method
Heat convection
Flow over a cylinder

ABSTRACT

An immersed-boundary method, previously developed for flow-field simulation, is extended to study heat-transfer problems of flow over a circular cylinder. The Dirichlet-type isothermal temperature boundary conditions and the Neumann-type iso-heat-flux boundary conditions are both implemented. To verify the accuracy of the simulation method, L_2-norm are computed to test the order of accuracy of the scheme. Numerical solutions are then further validated by comparing simulated temperature distributions and local convective-heat-transfer coefficients in flow over a stationary circular cylinder with data in the literature. Comparisons are made at different Reynolds-number flows and under different types of temperature boundary conditions. Finally, the effect of heat-transfer enhancement for flow over a transversely oscillating cylinder is investigated.

Published by Elsevier Inc.

1. Introduction

This paper describes an immersed-boundary-like approach to modeling and simulating heat-transfer problems with fluid–structure interactions. Because we are interested in forced-convection problems, the effect of buoyancy and compressibility are neglected. Therefore momentum and temperature equations are de-coupled and only one-way interaction from the momentum equations to the temperature equation is considered.

Immersed-boundary (IB) methods are typically designed for fluid–structure interaction problems. Almost all previously developed IB methods discretize the equations of motion for the fluid, i.e. Navier–Stokes equations. Peskin (1972) first developed the IB method to flow around the flexible leaflet of a human heart. More recent developments and reviews of this type of IB method have been discussed by Lai and Peskin (2000) and Peskin (2002). Goldstein et al. (1999) developed a feedback-force IB method for virtual boundary problems. Saiki and Biringen (1996) used this feedback-force IB method to calculate low Reynolds-number ($Re \leqslant 400$) flow over a stationary, rotating, and horizontally oscillating cylinder. They showed that the feedback-force IB method was capable of handling solid boundary problems, including moving boundaries. Feedback-force IB methods sometimes have severe stability problems and require two empirical constants in the force term. A new IB method, the direct-forcing IB method, was developed by Mohd-Yusof (1996). The force term generated in this manner directly compensates for the errors between the calculated velocities and the desired velocities on the boundary. With this method, the computation no longer suffers from stability limitations, and no empirical constants are needed to form the forcing term as in the scheme of Goldstein et al. (1999). Direct-forcing IB methods have been used successfully to simulate flow around spherical particles in particle-gas two-phase flow (Mohd-Yusof, 1996), 3-D complex-flow problems (Fadlun et al., 2000 and Mohd-Yusof, 1997), and flow with a moving object (Verzicco et al., 2000). Other direct-forcing methods incorporate different ways of treating IB conditions (Mittal and Iaccarino, 2005; Dong et al., 2006; Ravoux et al., 2003; Lima E Silva et al., 2003 and Tseng and Ferziger, 2003). But the typical direct-forcing IB method also suffers some drawbacks, such as complex treatments of the IB, and IB resolution dependence to the grid resolution. Zhang and Zheng (2007) developed an improved IB method which overcame drawbacks from both methods, and simulation results of flow over an oscillating cylinder were used to investigate the oscillating frequency and amplitude effects on lift and drag of the cylinder (Zheng and Zhang, 2008).

Although IB methods are widely used for fluid flow problems, few are used for heat-transfer problems. Kim and Choi (2004) and Tanno et al. (2006) applied the IB or IB-like methods to heat-transfer problems of flow over one or multiple cylinders. In both work, local Nusselt number distribution on the cylinder surface has been studied. However, only the Dirichlet-type isothermal IB condition has been implemented for the study of the convective-heat-transfer coefficient. Pacheco et al. (2005) implemented the IB method for incompressible flows with heat-transfer for both Dirichlet- and Neumann-type IB conditions. Their implementation was on a non-staggered grid and used a scheme similar to the direct-forcing method of Mohd-Yusof (1996), and thus inherited

* Corresponding author. Tel.: +1 337 475 5873.
E-mail address: nzhang@mcneese.edu (N. Zhang).

0142-727X/$ - see front matter. Published by Elsevier Inc.
doi:10.1016/j.ijheatfluidflow.2008.08.009

similar drawbacks. Pan (2006) introduced another recent IB implementation for heat-transfer problems. He used the volume-of-body (VOB) function to represent the temperature-immersed-boundary. But with VOB representation, the IB is not well conformed with the actual geometry, and the result shows a stair-step-like zigzag contour. Therefore, his method requires a very small grid size. No detailed study exists of local heat-transfer around the cylinder in the studies of Pacheco et al. (2005) and Pan (2006). Neither of these studies (Kim and Choi, 2004; Tanno et al., 2006; Pacheco et al., 2005; Pan, 2006) applied motion to the immersed object. Besides these implementations for solid-boundary problems, there have been several implementations for flexible-boundary problems, such as the study of heat-transfer for liquid droplet during deformation by Francois and Shyy (2003).

Numerous experimental and numerical studies of heat-transfer over a stationary circular cylinder have been conducted. Experimentally, Churchill and Bernstein (1977), Eckert and Soehngen (1952), and Roshko (1961) are among those. Numerically, studies from Momose and Kimoto (1999) and Bharti et al. (2007) are two with a similar Reynolds-number range compared to the present study. For the study of heat-transfer over an oscillating cylinder, literature data are relatively fewer. Experimentally, Sreenivasan and Ramachandran (1960) is among the earliest studies for the heat transfer from an oscillating cylinder in cross-flow. Due to the small oscillating frequencies used in their experiments, transverse oscillations had no effect on heat-transfer. Recently, Park and Gharib (2001) and Pottebaum and Gharib (2006) investigated the effects of transverse oscillations on the heat-transfer from a cylinder in cross-flow. However, no local heat-transfer-coefficient measurement was carried out in their research. Bouvier et al. (2005) describes an experimental study of heat-transfer in oscillating flow inside a cylindrical tube. Numerically, a finite element study was performed by Fu and Tong (2002) to study the flow structure and heat-transfer characteristics of a heated transversely oscillating cylinder in a cross-flow.

The purpose of this paper is to present an improved IB method for heat-transfer applications of incompressible fluid flow with constant properties, zero internal-heat generation, and negligible viscous heating effect. Note that the model is developed for applications with low-speed and low-viscosity fluid flows where viscous heating effects are very small. Viscous heating effects were initially included for several of the cases studies in this paper, and the results indicated that the viscous heating effects were indeed negligible. The present method adapts the IB approach of Zhang and Zheng (2007) for the motion of fluid flow and inherits such advantages: easy coding; independence of IB points to grid points, thus ensure the boundary conditions not only on the IB points intersecting with grid points, but also on the region in-between grid points; better conformation to the actual geometry; easy implementation with the weighting function; and increased accuracy without using higher-order schemes. Both Dirichlet-type isothermal and Neumann-type iso-heat-flux IB conditions were implemented. To verify the accuracy of the simulation method, heat conduction problems with analytical solutions were first computed. Numerical solutions were then further validated by comparing simulated temperature distributions and local convective-heat-transfer coefficients in flow over a stationary circular cylinder with data in the literature. Evidences of good agreement between the current results and previous literature data were found. Finally, the effect of heat-transfer enhancement for flow over a transversely oscillating cylinder was investigated. The present study also provides an understanding of the relationship between surface heat transfer and flow characteristics such as Reynolds number, vortex-shedding pattern, IB conditions, and motion of the immersed body.

2. Description of the IB method

In this paper, incompressible forced-convection problems are studied. The governing equations consists of Navier–Stokes equations and the temperature equation. The immersed-boundary is represented by momentum-forcing and energy-forcing terms. The focus of the paper is on energy-forcing and its treatments for different types of IB boundary conditions.

2.1. Governing equations and computational schemes

In the IB method, equations for unsteady incompressible fluid flow with constant properties, zero internal heat generation, and negligible viscous heating effect are

$$\nabla \cdot \mathbf{u} = 0, \tag{1}$$

$$\frac{\partial \mathbf{u}}{\partial t} + \mathbf{u} \cdot \nabla \mathbf{u} = -\nabla P + \frac{1}{Re}\nabla^2 \mathbf{u} + \mathbf{f_m}, \tag{2}$$

and

$$\frac{\partial T}{\partial t} + \mathbf{u} \cdot \nabla T = \alpha \nabla^2 T + f_e. \tag{3}$$

In the above equations, cylinder diameter D, free-stream velocity U_0, and density ρ are used for non-dimensionalization. Because of two different types of temperature boundary conditions are to be simulated, two different characteristic parameters are used to non-dimensionalize temperature. For the fixed surface-temperature boundary condition, temperature is non-dimensionalized using $(T_w - T_{inf})$, where T_w and T_{inf} are the cylinder surface-temperature and ambient temperature, respectively. For the fixed surface-heat-flux boundary condition, temperature is non-dimensionalized using $q_w D/k$, where k is the thermal conductivity, and q_w is the heat-flux on the cylinder surface. For insulated boundary conditions, temperature is non-dimensionalized using T_{inf} only. In Eq. (3), the parameter α, the inverse of the Peclet number, is defined as $1/PrRe$, where Pr and Re are the Prandtl number $c_p\mu/k$ and Reynolds number $U_0 D\rho/\mu$. In Eqs. (2) and (3), $\mathbf{f_m}$ and f_e are the momentum- and energy-forcing terms representing the virtual body force. Note the one-way interaction from velocity to temperature due to de-coupling between the momentum and energy equations.

Details of the computational scheme for the velocity field and determination of $\mathbf{f_m}$ have been shown by Zhang and Zheng (2007). The governing equations, Eqs. (1) and (2), are discretized using the first-order time-marching, with a semi-implicit term for the diffusion terms and the second-order Adams-Bashforth for convection and central differencing for diffusion. The procedure involves a two-step, predictor–corrector procedure. The two Poisson equations at each time step are solved using the Fishpack subroutines (1979) and Swarztrauber and Sweet (1979). Similarly for the temperature equation, Eq. (3) is also discretized using the first-order time-marching, with the second-order Adams-Bashforth for the convection terms and central differencing for the conduction terms.

The velocity predictor equation is

$$\mathbf{u}^* = \mathbf{u}^n + \delta t\left\{-\left(\frac{3}{2}\mathbf{S}^n - \frac{1}{2}\mathbf{S}^{n-1}\right) - \nabla P^* + \frac{1}{2Re}\nabla^2(\mathbf{u}^n + \mathbf{u}^*) + \mathbf{f_m}\right\}, \tag{4}$$

where ∇P^* is the pressure estimation

$$\nabla^2 P^* = -\nabla \cdot [(\mathbf{u}^n \cdot \nabla)\mathbf{u}^n - \mathbf{f_m}], \tag{5}$$

and $\mathbf{S}$ is the convection term defined as

$$\mathbf{S} = (\mathbf{u} \cdot \nabla)\mathbf{u}. \tag{6}$$

Then, with the following correction step, the real time velocity and pressure are given by:

$$\mathbf{u}^{n+1} = \mathbf{u}^* - \nabla\phi, \tag{7}$$

and

$$P^{n+1} = P^* + \phi, \tag{8}$$

where ϕ is the solution of the modified pressure Poisson equation (PPE)

$$\nabla^2\phi = \nabla\mathbf{u}^*. \tag{9}$$

The IB method is intended to use a force term to ensure correct velocity and temperature values on the boundary, in place of specifying the boundary conditions. The conservation laws are not altered in this method. Therefore, no additional special treatment is needed to enforce conservation laws at the boundary interface. A usual implementation of the governing equations, such as pressure correction ϕ in Eq. (9), is able to ensure the local conservation of mass (continuity).

The temperature equation at time step $n+1$ is

$$T^{n+1} = T^n + \delta t\left\{-\left(\frac{3}{2}\mathbf{S}_\mathbf{T}^n - \frac{1}{2}\mathbf{S}_\mathbf{T}^{n-1}\right) + \alpha\nabla^2 T^n + f_e\right\}, \tag{10}$$

where $\mathbf{S_T}$ is the convection term defined as

$$\mathbf{S_T} = (\mathbf{u}\cdot\nabla)T. \tag{11}$$

In the spirit of the IB method, IB points need not coincide with grid points. A bilinear interpolation (Saiki and Biringen, 1996) is used to determine the IB velocity and temperature $\mathbf{U}$ and T at one IB point, (x_s, y_s), surrounded by four grid points denoted by indices (i,j), $(i+1,j)$, $(i,j+1)$ and $(i+1,j+1)$

$$\mathbf{U}(\mathbf{x}_s) = \sum_{ij}^{i+1,j+1} D_{ij}(\mathbf{x}_s)\mathbf{u}_{ij}^n, \tag{12}$$

$$T(\mathbf{x}_s) = \sum_{ij}^{i+1,j+1} D_{ij}(\mathbf{x}_s)T_{ij}^n, \tag{13}$$

where the weighting function D is defined as

$$D_{ij}(\mathbf{x_s}) = d(x_s - x_i)d(y_s - y_i). \tag{14}$$

In Eq. (14), x_s and y_s are the x and y locations of the IB point, and

$$\begin{aligned} &d(x_s - x_i) = (x_s - x_{i+1})/(x_i - x_{i+1}) \quad \text{if } x_i < x_s,\\ &d(x_s - x_i) = (x_s - x_{i-1})/(x_i - x_{i-1}) \quad \text{if } x_i > x_s,\\ &d(x_s - x_i) = 1 \quad \text{if } x_i = x_s. \end{aligned}$$

It needs to be noted that this weighting function is not only used to calculate the IB velocity and force, but also used to determine the surrounding grid points to an IB point. This is because the function only has non-zero values as the distance between a grid point and an IB point is within one grid spacing.

The forcing terms, $\mathbf{f_m}$ and f_e, are designed to minimize the error at the boundary between the actual (computed) values at the new time and the desired (physical) values on the boundary surface, and they are non-zero only at a layer of grid points immediately inside the boundary with at least one neighbor in the fluid, named internal layer. The forcing terms are expressed as

$$\begin{aligned} \mathbf{f}_{\mathbf{m}(i,j)} = &\frac{1}{\delta t}\frac{1}{N_b}\sum_{n=1}^{N_b} D_{i,j}(\mathbf{x}_s)[\mathbf{V} - \mathbf{U}(\mathbf{x}_s)] + \left(\frac{3}{2}\mathbf{S}^n - \frac{1}{2}\mathbf{S}^{n-1}\right)_{i,j}\\ &- \frac{1}{Re}(\nabla^2\mathbf{u}^n)_{i,j} + \nabla P_{i,j}, \end{aligned} \tag{15}$$

$$\begin{aligned} f_{e(i,j)} = &\frac{1}{\delta t}\frac{1}{N_b}\sum_{n=1}^{N_b} D_{i,j}(\mathbf{x}_s)[T_w - T(\mathbf{x}_s)] + \left(\frac{3}{2}\mathbf{S}_\mathbf{T}^n - \frac{1}{2}\mathbf{S}_\mathbf{T}^{n-1}\right)_{i,j}\\ &- \alpha(\nabla^2 T^n)_{i,j}, \end{aligned} \tag{16}$$

where N_b is the number of IB points affecting the current grid point at (i,j), $\boldsymbol{V}$ and T_w are the desired boundary velocity and temperature, and $\mathbf{U}(\mathbf{x}_s)$ and $T(\mathbf{x}_s)$ are the computed boundary velocity and temperature. Note that T_w is a constant for Dirichlet boundary condition and changes with time and location for Neumann boundary condition. Since IB points do not necessarily coincide with the grid points, the computed boundary values are first interpolated from the grid points to the boundary points using Eqs. (12) and (13). Then in Eqs. (15) and (16), the differences between the desired boundary values and the computed boundary values are extrapolated back to the internal layer grid points, using the same bilinear weighting functions to determine the direct-forcing term.

Fig. 1 shows the interpolation and extrapolation between IB points and grid points near the IB. The IB value at one IB point, Point A, is determined by temperatures of those closest grid points (Points 1–4) using the weighting function, $D_{i,j}$. Then the IB forcing is mapped back to the internal layer instead of all grid points near the IB, as in the traditional feedback-force IB method (Saiki and Biringen, 1996). In Fig. 1, grid points having IB forcing applied are points 2 and 7–10, not all points from 1 to 10. This is to avoid numerical thickening of the boundary curve so that a sharp boundary interface can be achieved. From another point of view, the external layer is part of the flow-field and should not be "hardened" to be part of the boundary. Under this treatment, accuracy in the vicinity of the IB can be greatly improved, compared to traditional feedback-force methods.

The way that points 2 and 7–10 are selected is based on the weighting function $D_{i,j}$ in Eq. (14), as stated previously. From Eq. (14), if a grid point and an IB point are within one grid spacing, then $D_{i,j} > 0$, otherwise $D_{i,j} = 0$. All the grid points that satisfy this criterion are treated as the nearby grid points, which are points 1–10 in Fig. 1. And among those points that are interior to the boundary, points 2 and 7–10, are thus selected to apply the boundary force on.

As with all other direct-forcing IB methods, the IB resolution is determined by the grid resolution. Therefore, the resolution of the IB points are limited by the resolution of the grid lines near the boundary. With the interpolation procedure used in the current method, the points selected on the boundary (with locations denoted as $\mathbf{x}_s$) do not need to coincide with the grid points or intercepted points, as shown in Fig. 1. In order to increase the resolution on the boundary only, many more points (in fact, an arbitrary number of points) in between the intercepted points can be used to represent the IB points, and to be used later for extrapolating forcing back to the grid points. In this sense, the number of boundary points used, N_b, can be independently increased without being restricted to the resolution of the computational grid for the flow. For example, in Fig. 1, we can add another boundary point, Point B, other than Point A, but still be surrounded by the same group of

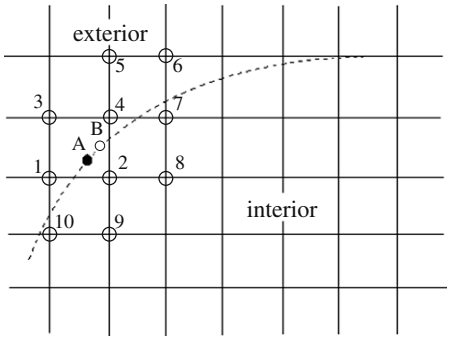

Fig. 1. Sketches showing interpolation/extrapolation between IB points and grid points near the IB.

grid points 1, 2, 3, and 4. Difference in values between Point A and Point B are due to the difference in weighting functions. By defining different weighting functions for different IB points to be used with the same group of grid points, many different boundary points can be added. With this procedure, influence of the IB surface can be better represented, because smoothness and accuracy of the IB surface can be independent of grid size. There are no limits on how many points can be distributed on the boundary. Of course, the increase of accuracy can reach a limit by adding boundary points without increasing computational grid resolution. However, within such a limit, local accuracy on the boundary can be improved by using more IB points to represent the boundary. A detailed study of the IB resolution requirement has been provided by Zhang and Zheng (2007). To prevent the information "leak" on the IB, the number of IB points should be at least two times the number of grid cells intercepted. In the current simulation cases, 960 IB points are used to represent the circular cylinder, which is about six times the number of intercepted grid cells with size of 0.025.

For direct-forcing methods, calculation of the force does not influence stability of time integration, as stated in (Fadlun et al., 2000). Therefore, the stability requirement for the temperature equation is based on a fully explicit scheme for a two-dimensional convection-diffusion equation (Ravoux et al., 2003). The time step needs to satisfy

$$\delta t < \min\left[\frac{h^2}{4\alpha}, \frac{2\alpha}{(u^2+v^2)}\right], \tag{17}$$

where h is the grid size. The first restriction in Eq. (17) is for conduction and the second restriction is for convection. Note that the stability requirement for momentum equations was discussed in (Zhang and Zheng, 2007), and is expressed as

$$\delta t < \min\left[\frac{h^2 Re}{4}, \frac{2}{(u^2+v^2)Re}\right]. \tag{18}$$

Similarly, the first restriction in Eq. (18) is for diffusion while the second for convection.

2.2. Dirichlet- and Neumann-type IB conditions

The specified IB temperature value is the desired boundary temperature T_w for the Dirichlet-type IB condition. It is uniform on the IB surface, and thus is called the isothermal condition. The difference between the specified temperature and the computed temperature constructs the IB forcing. Conceptually, all of the IB methods are originally designed for the Dirichlet-type boundary condition.

For the Neumann-type boundary condition problems, some manipulations of the boundary condition are necessary to apply the IB method. Since uniform heat-flux is specified instead of uniform temperature value on the boundary, the Neumann-type boundary condition is also called iso-heat-flux boundary condition in this study. For the iso-heat-flux boundary condition problems, T_w in Eq. (16) is not a constant and it has to be computed from the constant heat-flux. Heat flux is defined as $q = -(\mathrm{d}T/\mathrm{d}n)_{IB}$ = constant, thus the uniform heat flux is equivalent to the uniform normal temperature derivative. To deal with the normal temperature derivative, an additional layer of virtual points is defined, and is placed one-grid spacing (h) distance outside of the physical IB. The number of virtual points on the new layer is the same as the number of IB points. These two sets of points are aligned in the surface normal direction. Therefore, for any given pair of the IB and virtual points, the temperature derivative is defined as

$$-\left(\frac{\mathrm{d}T}{\mathrm{d}n}\right)_{IB} = \frac{T_w(\mathbf{x}_s) - T(\mathbf{x}_l)}{h}, \tag{19}$$

where $T_w(\mathbf{x}_s)$ and $T(\mathbf{x}_l)$ are the temperature values on the IB layer $\mathbf{x}_s$ and the additional virtual layer $\mathbf{x}_l$. Temperature values of the virtual layer points are computed using the same interpolation as in Eq. (13) for IB temperature calculations. For the Neumann-type IB condition, temperature values on every IB point need to satisfy the relation in Eq. (19) at any given moment. So the desired IB T_w in Eq. (16) at time $n+1$ is determined by

$$T_w(\mathbf{x}_s)^{n+1} = -h\left(\frac{\mathrm{d}T}{\mathrm{d}n}\right)_{IB} + T(\mathbf{x}_l)^n. \tag{20}$$

Note that $-(\mathrm{d}T/\mathrm{d}n)_{IB}$ is the specified heat-flux. Unlike the Dirichlet-type IB condition, the desired IB T_w in Neumann-type IB condition changes with time and location.

From Eq. (16), the values of internal layer points on which the forcing are applied, are the forced values to enable the desired IB values. This layer is a boundary shared by both interior and exterior domains. From the nature of the present method, the internal layer acts as a shield layer preventing communication between further interior points and exterior points. With this shield layer, the artificial interior region, sometimes with unrealistic data values, does not influence the physical exterior domain. For example, with heat-flux across the IB surface, there might be unwanted heat accumulation in the interior region. But with the present method, as long as the internal layer is well defined, the solutions outside the IB surface are not affected by the unreal interior solutions. This is another major advantage of the direct-forcing type of IB methods.

For both types of boundary conditions, the local Nusselt number around the cylinder surface is defined as HD/k, where H is the local heat-transfer coefficient. In this study, it is calculated based on nondimensionalization. For the isothermal boundary condition, it is expressed as

$$Nu_{local} = -\frac{\mathrm{d}T}{\mathrm{d}n}, \tag{21}$$

where n is the normal direction from the cylinder surface. In the calculation of surface derivative $\mathrm{d}T/\mathrm{d}n$, again, the additional layer of points one-grid spacing outside the cylinder is defined and their differences to the surface values divided by the distance are the $\mathrm{d}T/dn$ values. For the iso-heat-flux boundary condition, the local Nusselt number on the cylinder surface is

$$Nu_{local} = \frac{1}{T}, \tag{22}$$

where T is the dimensionless surface-temperature interpolated using Eq. (13).

3. Results and discussion

In this section, convection heat-transfer problems are simulated using the IB method presented in the previous section. Heat convection with flow over a stationary or oscillating cylinder are selected as the target cases. The simulation results are compared with results from previous experimental and numerical studies in the literature. Isothermal and iso-heat-flux IB conditions are implemented and studied. In this paper, the Reynolds-number range is from 20 to 218. The Prandtl number is fixed at 0.7 for all cases. The staggered grid arrangement is applied for all convection cases in this paper. Cylinder diameter D is 1, as well as the free-stream velocity U_0. The computational domain size is 25.6×12.8, with the center of the cylinder located at (6.4, 6.4). For boundary conditions at the inlet, $u = 1$, $v = 0$, and $\partial P/\partial x = 0$ are prescribed. On the top and bottom boundaries, $\partial u/\partial y = 0$, $v = 0$, and $\partial P/\partial y = 0$ are imposed. At the outlet, the two velocity components are assumed to have zero-normal derivatives, $\partial u/\partial x = 0$ and $\partial v/\partial x = 0$, and $P = 0$. Although the outlet boundary condition is not a strict

non-reflecting boundary condition, from the simulation results, it seems to successfully convect large vortical structures out of the domain without any reflection. Current pressure boundary conditions at the inlet and outlet boundaries are imposed to be consistent with the equations for the velocities, due to the staggered grid arrangement (Ravoux et al., 2003). For temperature at the inlet, $T = 0$ is specified. At the other three boundaries, the zero-normal derivative is specified. On the cylinder surface, $T_w = 1$ is specified for isothermal cases, while $q_w = 1$ is specified for iso-heat-flux cases. Because of the one-way interaction between velocity field and temperature field, the accuracy of temperature field does not influence velocity and pressure computations. The velocity and pressure fields for flow over a stationary or oscillating cylinder have been validated previously at this Reynolds-number range (Zhang and Zheng, 2007). Therefore, the validation in this paper is for temperature only. Based on the stability requirements of Eqs. (17) and (18), time steps are in the range of 0.001–0.01.

3.1. Verification of the numerical scheme

Grid-size independence tests have been performed to verify the numerical scheme. The stationary cylinder case with $Re = 20$ is selected for the tests. There are four levels of grid sizes: coarsest, coarse, fine, and finest. The grid size of each level is 0.1, 0.05, 0.025 and 0.0125, respectively. Temperature values along the x-axis, starting from the point on the cylinder surface at (6.9,6.4) to the end of the domain, are used for the comparison among different grid levels. Norms of relative errors of temperature distributions are indicatives of accuracy of the scheme when the grid size changes. Fig. 2 shows the L_2-norm of all the temperature values along the x-axis. Regarding the solution on the finest grid as "exact", the errors of the solution are computed on the coarser grids. From Fig. 2, for both types of boundary conditions, we find when changing the grid resolution, the norm shows a "−2" slope in the log–log plot of the norm versus the grid number. This indicates that the overall computational accuracy is second order in space, and a grid size of 0.025 is sufficiently fine for temperature simulation. The grid-independence study was performed previously for the fluid-flow simulation (Zhang and Zheng, 2007), and a second-order accuracy was also obtained when the same 0.025 grid size was selected. Therefore, for all the results shown in this paper, the grid size of 0.025 is used.

3.2. Heat convection with flow over a stationary cylinder

Numerical solutions of low-Reynolds-number flow over a stationary cylinder is validated first. According to Zdravkovich (1997), at the low-Reynolds-number range of $Re \leqslant 50$ the vortex structure in the wake is steady and symmetric, thus the temperature field shows similar steady and symmetric characteristics. In the low-Reynolds-number range, $Re = 20$ is selected for the study. The local Nusselt numbers on the cylinder surface are calculated and compared with the literature data.

Present results of Nusselt number distribution on the cylinder surface are compared with recent numerical results from Bharti et al. (2007), and the comparisons are shown in Fig. 3. It can be seen that the two sets of data are very close. Although Nusselt number distributions in the isothermal and iso-heat-flux cases are different, the patterns are similar with the two different types of boundary conditions. The largest Nusselt number is located at the front stagnation point of the cylinder; then the Nusselt number decreases continuously to the rear stagnation point, with more significant decrease in the isothermal case. For both of the cases, the Nusselt numbers reach the lowest value at the rear stagnation point. Also at the rear stagnation point, the difference between the two boundary conditions is the maximum. This Nusselt number distribution is related to the velocity distribution around the surface where higher velocity leads to a higher heat-transfer coefficient. On the other hand, differences in the Nusselt number between isothermal and iso-heat-flux boundary conditions are due to differences of temperature distribution on the cylinder surface. Therefore, along the cylinder surface, convective-heat-transfer coefficients are mostly higher for the iso-heat-flux case, especially at the rear portion of the cylinder surface.

At larger Reynolds numbers ($Re \geqslant 50$), there is an unsteady wake in the velocity field, i.e., the von Karman vortex sheet shed from the cylinder surface. Because of the velocity field, a similar shedding pattern also takes place in the temperature field. In the unsteady cases, the time-averaged Nusselt number is used in the discussion below. In this laminar Reynolds-number range, two

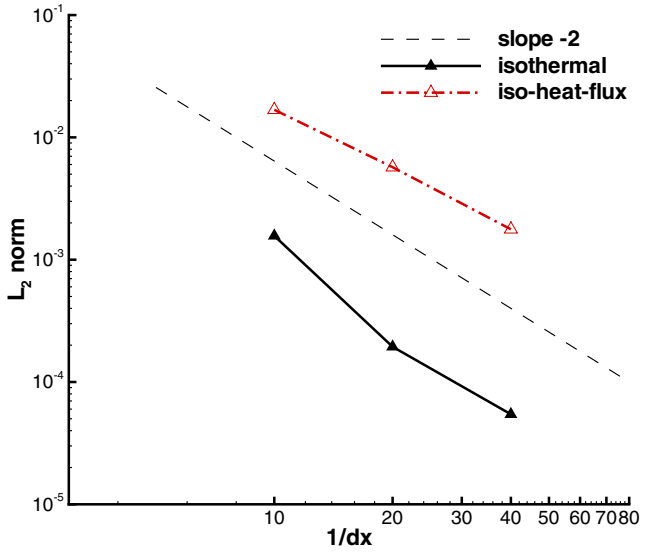

Fig. 2. The L_2-norm of the temperature along the axis versus the grid number per cylinder diameter for steady case with $Re = 20$, with two types of boundary conditions.

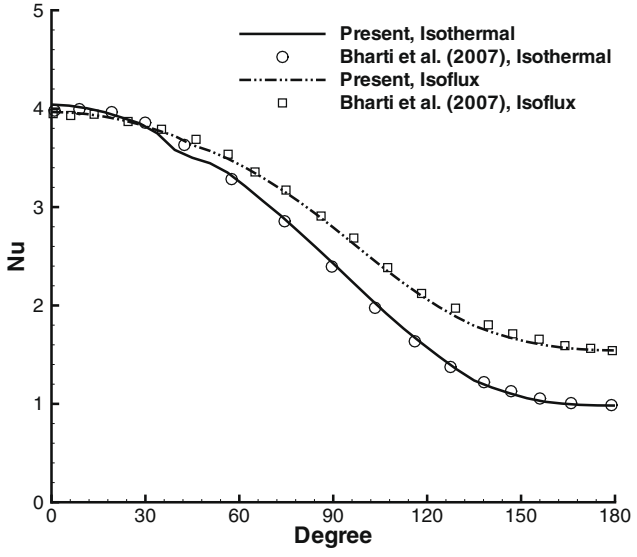

Fig. 3. Comparisons of local Nusselt number distributions on the cylinder surface between present results and results in the literature for the case with $Re = 20$. The angle, θ, is defined in the clockwise sense starting from the surface point at (5.5,6.4).

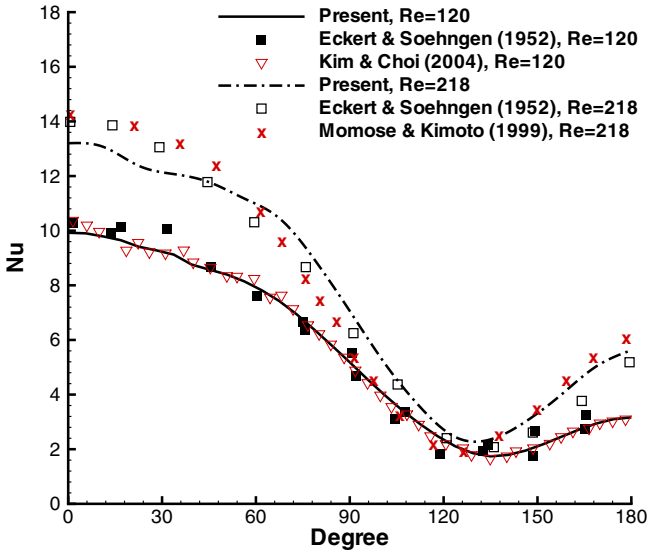

Fig. 4. Comparisons of local Nusselt number distributions on the cylinder surface between present results and results in the literature for the cases with Re = 120,218 and isothermal IB conditions. The angle is defined in the same way as in Fig. 3.

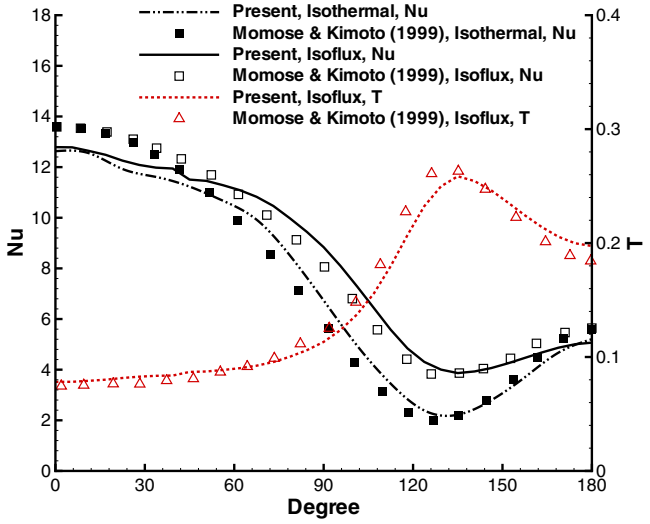

Fig. 5. Comparisons of local Nusselt number and temperature distributions on the cylinder surface between present results and results in the literature for the case with Re = 200, with two different types of boundary conditions (where the temperature distribution comparison is for the iso-heat-flux boundary condition only).

issues are interesting: one is the relation between Nusselt number and Reynolds number; the other is the relation between Nusselt number and the types of IB conditions. Again, the former relation is decided by the flow velocity, while the later is related to surface-temperature distribution.

The influence of Reynolds number on Nusselt number is shown in Fig. 4, where surface Nusselt number distributions for two cases with Re = 120 and 218 are plotted. The comparisons are made among present results, experimental results from Eckert and Soehngen (1952), and previous numerical results from Kim and Choi (2004) and Momose and Kimoto (1999). The boundary condition is isothermal. For the Re = 120 case, the present result matches well with both literature data. For the Re = 218 case, the present result under-predicts the Nusselt number on the front portion of the surface, then compares better afterwards with the experimental data than the result of Momose and Kimoto (1999). Overall, the Nusselt number increases with the increase of Reynolds number because of the higher flow velocity. In Fig. 4, the minimum Nusselt number values are about the same for the two Reynolds number cases and occur at about 130°, near the flow separation point. Unlike the steady state case, after this point, the Nusselt numbers increase as they approach the rear stagnation point. This is the major difference in the pattern of surface Nusselt number distribution compared to the steady case, which is due to the formation of vortex shedding that causes higher velocity near the rear part of the cylinder. Compared to the steady case of Re = 20 in Fig. 3, the overall Nusselt number increase in Fig. 4 is due to the higher velocity of the larger Reynolds number. The difference in the rear portion of the cylinder surface between Figs. 3 and 4 is because of vortex shedding in the high Reynolds number cases.

Effects of two boundary conditions on Nusselt number are shown in Fig. 5 for the case of Re = 200. The present surface Nusselt number and temperature results are compared with the results of Momose and Kimoto (1999), and the overall agreement is good. The two sets of data show that the Nusselt numbers are the same at the front stagnation point for the two different boundary conditions. The two curves are separated towards downstream. It is clear that the Nusselt numbers of the iso-heat-flux cases are larger than those of the isothermal cases, which indicates a better convective-heat-transfer with iso-heat-flux boundary conditions. The location of the maximum differences between isothermal and iso-heat-flux Nusselt number curves is at the flow separation point, instead of at the rear stagnation point as in the steady case of Re = 20. Downstream of that location, the Nusselt numbers of both boundary conditions increase, gradually getting closer to each other when approaching the rear stagnation point and finally matching. Fig. 5 also shows in the iso-heat-flux cases, the Nusselt number increases as the surface-temperature decreases. On the front surface, the Nusselt numbers are relative higher, resulting in the lower surface-temperature, while it is the opposite on the rear surface. This inverse trend between Nusselt number and temperature also matches the results of Momose and Kimoto (1999). In addition, with the same Reynolds number, differences in heat-transfer between two boundary conditions are due to differences in surface-temperature distributions.

Fig. 6 is the plot of overall Nusselt number on the cylinder surface versus Reynolds number. The comparisons are between

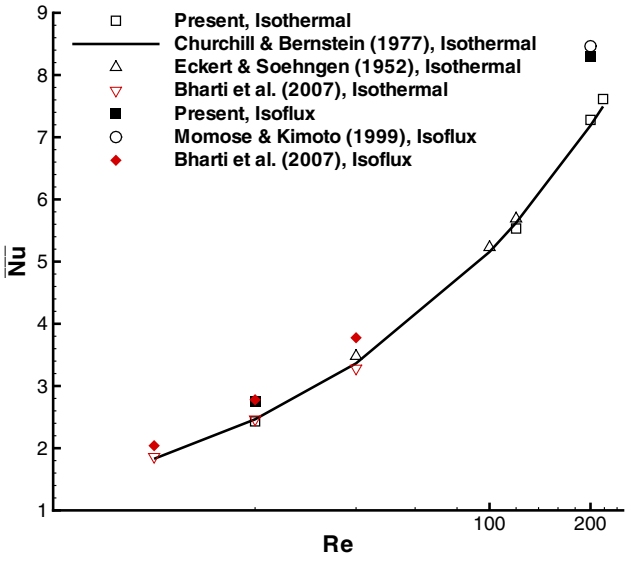

Fig. 6. Comparisons of mean Nusselt number versus Re between present results and results in the literature.

present results and previous experimental and numerical results, and the agreement is good. The heat-transfer increases with the increase of Reynolds number. Unsteady cases are better than steady cases in heat-transfer because of higher flow velocity and existence of vortex shedding that transfers more heat from the cylinder surface. For the unsteady cases, heat transfer of a higher Reynolds number flow is better because the velocity is higher and the vortex shedding is faster. For the same flow, effectiveness of heat-transfer is also affected by the boundary conditions, with iso-heat-flux boundary conditions leading to better heat-transfer.

3.3. Heat convection with flow over an oscillating cylinder

Because of the immersed-boundary method used in this research, we are able to simulate flow over an oscillating cylinder with little extra computational cost. The purpose is to study the improvement of heat transfer due to oscillating motion. Reynolds number of 200 is selected. The setups are the same as for the stationary cylinder cases. The oscillation is in the cross-flow direction, and has the dimensionless displacement of

$$d_y = A\sin(2\pi ft), \tag{23}$$

where A is the dimensionless amplitude of the oscillating displacement selected between 0.15 and 0.4, and f is the dimensionless oscillating frequency. In this study, $f = 0.2$ is chosen, which is the same value as the natural vortex-shedding frequency. The motion described in the above equation is applied to all immersed boundary points and there is no motion in the x direction. The fidelity of the flow-field for the oscillating cases has been previously verified (Zhang and Zheng, 2007). Particularly, the computational results of fluctuation quantities have been compared with experimental data by Griffin (1971), and a very good agreement between two results has been achieved, as shown in the paper (Zhang and Zheng, 2007).

Fig. 7 shows a snapshot of the temperature distribution for one oscillating case with the isothermal boundary condition and $A = 0.15$. Note that, there can be temperature values inside the cylinder because of the IB method used. The inside values are all greater than one in this case, thus not shown in the figure because they exceed the contour-value range. It shares a similar pattern with the other oscillating cases, including those with iso-heat-flux boundary conditions. It should be pointed out that this temperature distribution is also similar to that of the stationary case, because the use of the natural shedding frequency as the oscillating frequency leads to a similar vortex-shedding pattern. The snapshot is at dimensionless time 100, and the cylinder is at the middle location during its upward motion cycle. It is also observed that the temperature distribution pattern is similar to the vortex-shedding pattern shown in the paper (Zhang and Zheng, 2007), which provides an evidence that heat-transfer from the cylinder surface is mostly determined by the vortex shedding in the flow.

Fig. 8 is the comparisons of surface Nusselt number distributions between present results and results from Fu and Tong (2002). In this case, $Re = 200$ and $A = 0.4$. The comparisons are at

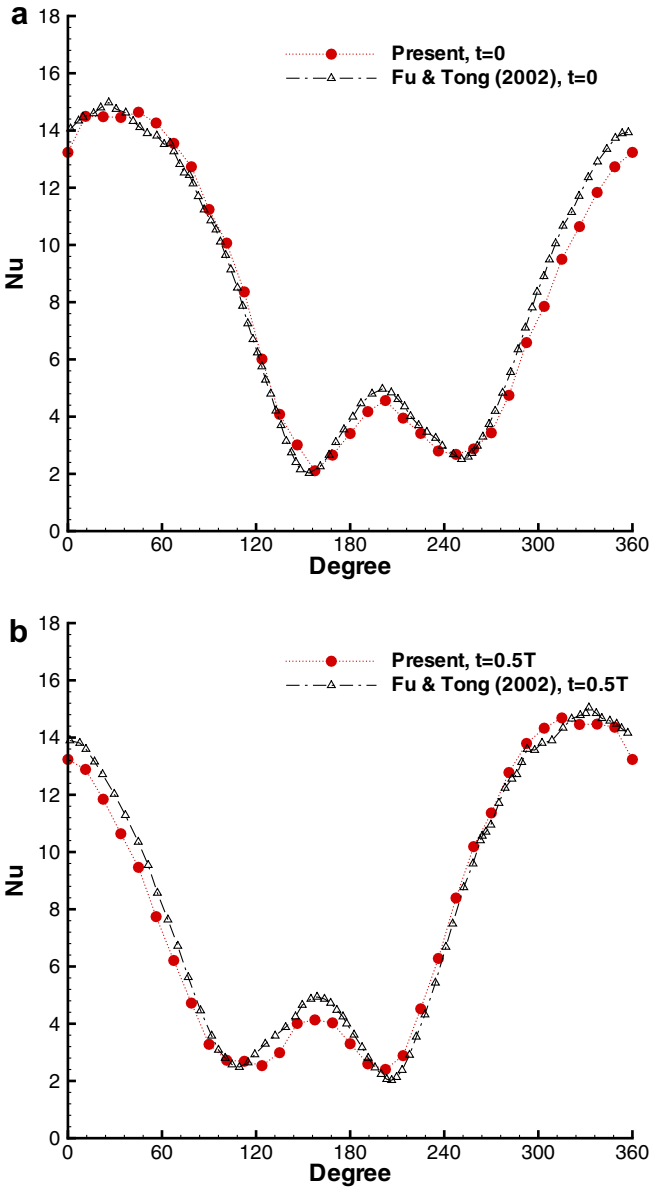

Fig. 8. Comparisons of local Nusselt number distribution on the cylinder surface between present results and results in the literature for the oscillating cylinder case with $Re = 200$, at two different time: (a) $t = 0$, (b) $t = T/2$.

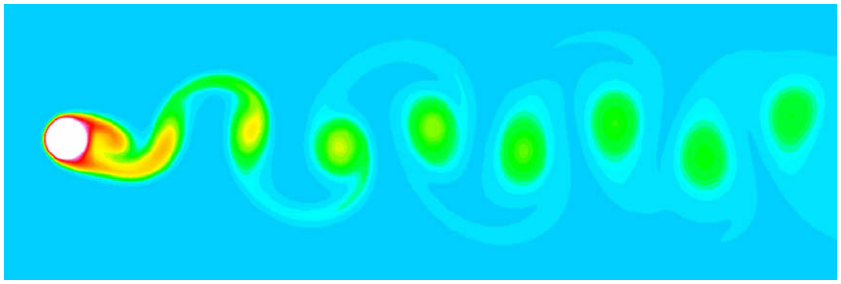

Fig. 7. Temperature distribution contours for the oscillating cylinder case with $Re = 200$.

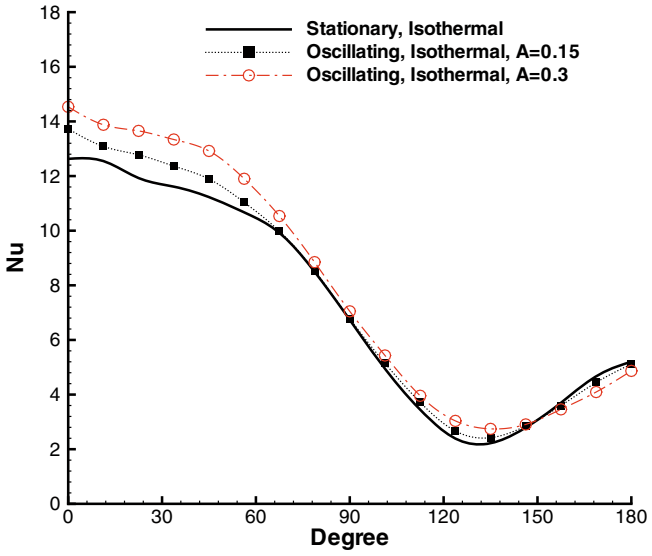

Fig. 9. Comparisons of local Nusselt numbers between stationary and oscillating cylinder cases with $Re = 200$ for isothermal temperature boundary conditions.

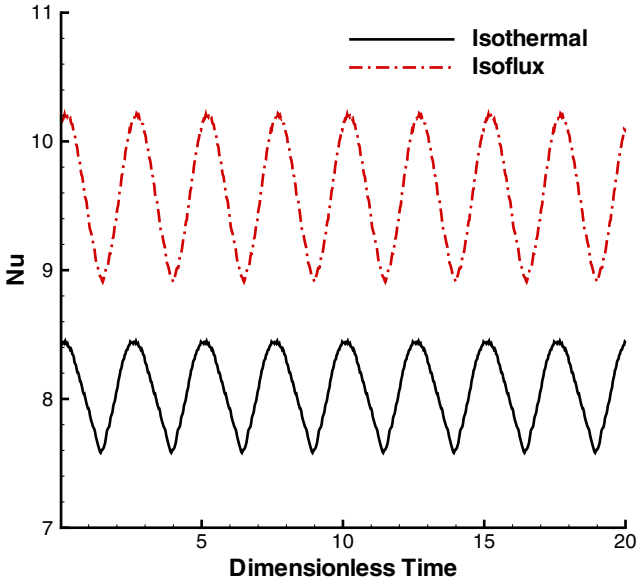

Fig. 11. Time histories of surface-averaged Nuseelt numbers for the oscillating cylinder case with $Re = 200$ and $A = 0.3$ for both of the isothermal and iso-flux cases.

two instances during an oscillating period. One is at $t = 0$ when the cylinder moves upward with maximum speed; the other is at the time of half period when the cylinder moves downward with maximum speed. The agreement between the two results are good. The maximum heat-transfer occurs at the region a little above the front stagnation point when the cylinder moves upward, and at the region a little below the front stagnation point when it moves downward (see Fig. 8). The maximum heat-transfer is due to the maximum flow velocity at that region. The minimum heat-transfer occurs near the flow separation point where a vortex sheds from the surface. Figs. 9 and 10 are comparisons of surface Nusselt number and temperature between oscillating and stationary cases, for each type of boundary conditions, respectively. These figures show that oscillating motion improves surface heat-transfer for both types of temperature boundary conditions, and the improvement increases as oscillating amplitude increases. This agrees with observations of Pottebaum and Gharib (2006). The improvement

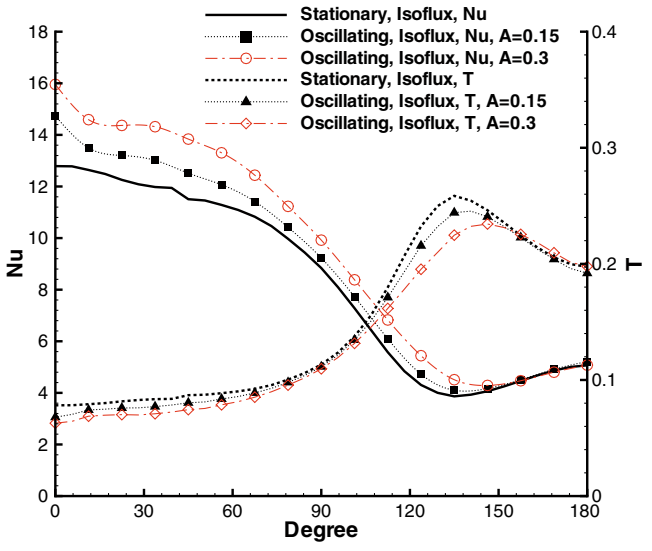

Fig. 10. Comparisons of local Nusselt numbers and temperature distribution between stationary and oscillating cylinder cases with $Re = 200$ for iso-heat-flux boundary conditions.

is mostly at the front surface of the cylinder. This is because heat transfer at the front surface is due to flow velocity, while it is mostly due to vortex shedding at the rear surface. The oscillating motion increases the velocity at the front surface, but does not change much the shedding pattern at the rear surface. The improvement is slightly larger with the iso-heat-flux boundary condition. For the iso-heat-flux cases, the inverse trend between surface-temperature and Nusselt number, as shown in stationary cylinder cases in Fig. 7, can also be observed. In comparing the two boundary conditions for oscillating cases, again, iso-heat-flux is better in heat-transfer, similar to that in the stationary cases.

The time histories of overall (surface-averaged) Nusselt numbers are shown in Fig. 11 for the case of $Re = 200$ and $A = 0.3$. It has been found that in many of the previous IB methods, overall Nusselt number histories have kinks when IB points stride grid lines on a Cartesian grid mesh in moving boundary problems. The present results in Fig. 11 indeed show the small kinks in the histories due to IB points striding grid lines, but the magnitudes of these kinks are very small. Notice that the shapes of the top and bottom peaks are slightly different. The reason is that, within one oscillating period of dimensionless time 5, there are two top peaks, each occurring when the cylinder moves across the middle location, while the two bottom peaks occur when the cylinder reaches the highest and lowest locations. Therefore, the curves still show the symmetrical heat-transfer feature with respect to the up-and-down oscillating motion due to the symmetrical vortex shedding.

4. Conclusions

The IB method for heat-transfer applications developed in this paper is based on a previously validated IB method for fluid flow (Zhang and Zheng, 2007), thus it inherits the same advantages over other IB methods. The strong points of the present method are: (1) number of IB points independent of grid resolution to ensure the boundary condition not only on the IB locations intersecting with grid points, but also on the region in-between grid points; (2) easy implementation with the weighting functions; (3) less kinks and smoother curves in the overall Nusselt number histories when IB points striding the grid lines on a Cartesian grid mesh. These

advantages result in an IB method that is more accurate and easier to implement than other methods. Comparing present results with the experimental and numerical data in literature, good agreements have been found. In particular, the fact that the present IB method successfully treats Neumann-type IB conditions and moving boundary problems provides a strong evidence for the capability of this method.

For the problem of flow over a circular cylinder, the Nusselt number increases with the increase of Reynolds number. The increase is mostly due to the higher flow velocity and stronger vortex shedding. Between steady and unsteady cases, the Nusselt number distributions show different patterns because of the presence of the vortex shedding in the unsteady cases. Between two types of boundary conditions, the iso-heat-flux condition is better in heat-transfer than the isothermal condition for the same Reynolds number. The reason is the difference in surface-temperature distributions. On an iso-heat-flux boundary, the surface-temperature changes inversely with the Nusselt numbers. When applying oscillating motion to the cylinder, heat-transfer always improves, and the improvement increases as the oscillating amplitude increases. The region with the most improvement is the front surface, because of the increase of flow velocity due to motion. At the rear surface, the similar shedding pattern between stationary and oscillating cases leads to an insignificant improvement when the oscillating frequency is the natural vortex-shedding frequency.

References

Bharti, R.P., Chhabra, R.P., Eswaran, V., 2007. A numerical study of the steady forced convection heat transfer from an unconfined circular cylinder. Heat Mass Transfer 43, 639–648.

Bouvier, P., Stouffs, P., Bardon, J.P., 2005. Experimental study of heat transfer in oscillating flow. Int. J. Heat Mass Transfer 48, 2473–2482.

Churchill, S.W., Bernstein, M., 1977. A correlating equation for forced convection from gases and liquids to a circular cylinder in crossflow. J. Heat Transfer 99, 300–306.

Dong, H., Mittal, R., Najjar, F.M., 2006. Wake topology and hydrodynamic performance of low-aspect-ratio flapping foils. J. Fluid Mech. 566, 309–343.

Eckert, E.R.G., Soehngen, E., 1952. Distribution of heat-transfer coefficients around circular cylinders in crossflow at Reynolds numbers from 20 to 500. Trans. ASME 75, 343–347.

Fadlun, E.A., Verzicco, R., Orlandi, P., Mohd-Yusof, J., 2000. Combined immersed-boundary finite-difference methods for three dimensional complex flow simulations. J. Comp. Physiol. 161, 35–60.

Francois, M., Shyy, W., 2003. Computations of drop dynamics with the immersed boundary method. Numer. Heat Transfer, Part B 44, 101–143.

Fu, W.S., Tong, B.H., 2002. Numerical investigation of heat transfer from a heated oscillating cylinder in a cross flow. Int. J. Heat Mass Transfer 45, 3033–3043.

Goldstein, D., Handler, R., Sirovich, L., 1999. Modeling a no-slip flow boundary with an external force field. J. Comp. Physiol. 105, 354–366.

Griffin, O.M., 1971. The unsteady wake of an oscillating cylinder at low Reynolds number. J. Appl. Mech. 38, 729–738.

Kim, J., Choi, H., 2004. An immersed-boundary finite-volume method for simulation of heat transfer in complex geometries. Korean Soc. Mech. Eng. Int. J. 18 (6), 1026–1035.

Lai, M.C., Peskin, C.S., 2000. An immersed boundary method with formal second-order accuracy and reduced numerical viscosity. J. Comp. Physiol. 160, 705–719.

Lima E Silva, A.L.F., Silveira-Neto, A., Damasceno, J.J.R., 2003. Numerical simulation of two-dimensional flows over a circular cylinder using the immersed boundary method. J. Comp. Physiol. 189, 351–370.

Mittal, R., Iaccarino, G., 2005. Immersed boundary method. Ann. Rev. Fluid Mech. 37, 239–261.

Mohd-Yusof, J., 1996. Interaction of Massive Particles with Turbulence. Ph.D. thesis. Cornell University.

Mohd-Yusof, J., 1997. Combined immersed-boundary/B-spline methods for simulations of flow in complex geometries. Annual Research Briefs, Center for Turbulence Research, pp. 317–327.

Momose, K., Kimoto, H., 1999. Forced convection heat transfer from a heated circular cylinder with arbitrary surface temperature distributions. Heat Transfer-Asian Res. 28 (6), 484–499.

Pacheco, J.R., Pacheco-Vega, A., Rodic, T., Peck, R.E., 2005. Numerical simulation of heat transfer and fluid flow problems using an immersed-boundary finite-volume method on nonstaggered grids. Numer. Heat Transfer, Part B 48, 1–24.

Pan, D., 2006. An immersed boundary method on unstructured Cartesian meshes for incompressible flows with heat transfer. Numer. Heat Transfer, Part B 49, 277–297.

Park, H.G., Gharib, M., 2001. Experimental study of heat convection from stationary and oscillating circular cylinder in cross flow. J. Heat Transfer 123, 51–62.

Peskin, C.S., 1972. Flow patterns around heart valves: a numerical method. J. Comp. Physiol. 10, 252–271.

Peskin, C.S., 2002. The immersed boundary method. Acta Numer. 11, 479–517.

Pottebaum, T.S., Gharib, M., 2006. Using oscillations to enhance heat transfer for a circular cylinder. Int. J. Heat Mass Transfer 49, 3190–3210.

Ravoux, J.F., Nadim, A., Haj-Hariri, H., 2003. An embedding method for bluff body flows: interactions of two side-by-side cylinder wakes. Theor., Comput. Fluid Dynam. 16, 433–466.

Roshko, A., 1961. Experiments on the flow pass a circular cylinder at very high Reynolds number. J. Fluid Mech. 10, 345–356.

Saiki, E.M., Biringen, S., 1996. Numerical simulation of a cylinder in uniform flow: application of a virtual boundary method. J. Comp. Physiol. 123, 450–465.

Sreenivasan, K., Ramachandran, A., 1960. Effect of vibration on heat transfer from a horizontal cylinder to a normal air stream. Int. J. Heat Mass Transfer 3, 60–67.

Swarztrauber, P.N., Sweet, R.A., 1979. Algorithm 541, efficient FORTRAN Subprograms for the solution of separable elliptic partial differential equations [D3]. ACM Trans. Math. Software 5, 352–364.

Tanno, I., Morinishi, K., Matsuno, K., Nishida, H., 2006. Validation of virtual flux method for forced convection flow. JSME Int. J. 49, 1141–1148.

Tseng, Y.H., Ferziger, J.H., 2003. A ghost-cell immersed boundary method for flow in complex geometry. J. Comp. Physiol. 192, 593–623.

Verzicco, R., Mohd-Yusof, J., Orlandi, P., Haworth, D., 2000. Large eddy simulation in complex geometric configurations using boundary body forces. AIAA J. 38 (3), 427–433.

Zdravkovich, M.M., 1997. Flow Around Circular Cylinder. Oxford University Press.

Zhang, N., Zheng, Z.C., 2007. An improved direct-forcing immersed-boundary method for finite difference applications. J. Comp. Physiol. 221, 250–268.

Zheng, Z.C., Zhang, N., 2008. Frequency effects on lift and drag for flow past an oscillating cylinder. J. Fluid. Struct. 24(3).